Eurasian Journal of Science Engineering and Technology

Research Article

INVESTIGATION OF STRUCTURAL, OPTICAL, AND ELECTRICAL PROPERTIES OF ITO FILMS DEPOSITED AT DIFFERENT PLASMA POWERS: ENHANCED PERFORMANCE AND EFFICIENCY IN SHJ SOLAR CELLS

Emre KARTAL [1 *], İlker DURAN [2], Elif DAMGACI [3] Ayşe SEYHAN [4]

[1,2,3,4] *Nigde Omer Halisdemir University, Nanotechnology Research Center, 51240, Nigde, Türkiye*
[1,4] *Nigde Omer Halisdemir University, Department of Physics, 51240, Nigde, Türkiye*
[3] *Nigde Omer Halisdemir University, Department of Mechanical Engineering, 51240, Nigde, Türkiye*

ABSTRACT

This article presents an investigation into the structural, optical, and electrical properties of Indium Tin Oxide (ITO) films that were deposited utilizing various plasma powers. The transmittance values in the visible region were measured, revealing that the ITO film deposited at 2050 W exhibited the highest transmittance (81%). Additionally, the sheet resistance values of all films were analyzed, indicating that the ITO film deposited at 2050 W had the lowest sheet resistance (64.9 Ω/sq). By means of XRD analysis, the structural properties of the films were meticulously scrutinized, and the distinctive diffraction peaks associated with the ITO films were successfully identified. Notably, the ITO film deposited at 2050 W demonstrated superior performance compared to the other films deposited using various plasma powers. Finally, we report a noteworthy efficiency of 17.03% achieved in the SHJ solar cell fabricated with the ITO film deposited at 2050 W on a 5x5 cm^2 n-type Si substrate.

Keywords: Transparent conductive oxide (TCO), Indium Tin Oxide (ITO), DC magnetron sputtering, Sheet resistance, Optical transmittance

1. INTRODUCTION

Solar energy holds significant potential as a renewable energy source, and recent advancements in technology coupled with cost reductions have made it even more promising. Various solar cells utilizing different materials have been developed, and among them, crystalline silicon (c-Si) solar cells have gained widespread use in photovoltaic (PV) technology for several decades. These c-Si solar cells offer advantages such as an optimal band gap, high efficiency, and easy access to raw materials [1]. Among the array of c-Si-based solar cell technologies, heterojunction solar cells utilizing c-Silicon (SHJ cells) have arisen as the preeminent choice in terms of efficiency. SHJ solar cells have garnered considerable interest due to their affordability, low deposition temperatures (<200°C), high efficiency, and simplified fabrication processes [2]. In recent years, remarkable conversion efficiencies of 25.6% and 26.7% have been achieved in SHJ solar cells [3], [4].

Transparent Conductive Oxide (TCO) layers play a critical role in SHJ due to their multifaceted significance and essential functionalities. These layers play a pivotal role in generating electron-hole pairs, facilitating the transmission of incoming light to the p-n junction, and minimizing reflection [5]. Furthermore, the integration of TCO layers is imperative to ensure efficient current collection in SHJ, primarily due to the elevated resistance exhibited by a-Si:H layers and the constrained lateral conductivity of p-doped a-Si:H layers. The utilization of TCO materials extends beyond the domain of SHJ and holds notable importance in a wide range of other devices, including but not limited to light-emitting diodes (LEDs) [6], dielectric transistors [7], flexible electronics [8], fuel cells [9], as well as in ubiquitous consumer electronics such as smartphones, monitors, and flat panel displays [10].

The production of TCO layers involves employing a diverse array of techniques, including but not limited to chemical vapor deposition (CVD) [11], pulsed laser deposition [12], physical vapor deposition (PVD) [13], [14], ion-assisted plasma evaporation [15], electron beam evaporation [16], direct current (DC) [17], radio frequency (RF) magnetron sputtering [18], and thermal evaporation [19]. Magnetron sputtering is a commonly employed technique in the production of TCO layers, primarily due to its favorable manufacturing characteristics. These include the ability to maintain excellent optoelectronic performance of the film [20], [21], while enabling industrial field applications through features like low substrate temperatures and high deposition rates. Furthermore, magnetron sputtering is favored for its capability to yield films with superior electrical and optical properties, as well as ensuring good surface homogeneity.

Indium tin oxide (ITO) [22], aluminum zinc oxide (AZO) [23], indium tungsten oxide (IWO) [24], indium zinc oxide (IZO) [25], and fluorine tin oxide (FTO) [26] are among the commonly employed TCOs today. ITO, specifically, is composed of a

* Corresponding author, e-mail: emrekartal4271@gmail.com (E. Kartal)
Recieved: 16.05.2023 Accepted: 25.05.2023
doi: 10.55696/ejset.1297942

solid compound consisting of indium (III) oxide (In_2O_3) and tin (IV) oxide (SnO_2), typically with a composition of 90% In_2O_3 and 10% SnO_2. Its application in solar cells is widespread due to its satisfactory conductivity and permeability performance [27]. When employed as a thin film, ITO demonstrates favorable characteristics as a viable option for a conductive layer, owing to its diminished surface resistance and enhanced permeability in comparison to alternative materials currently available. Moreover, ITO serves as an n-type semiconductor material with a discernible direct band gap spanning from 3.5 to 4.3 eV [28]. This distinctive property exerts a notable influence on the morphological, optical, and electrical attributes of ITO, consequently facilitating the fabrication of materials characterized by exceptional performance [29], [30].

In this research, a series of ITO films were deposited on 5x5 cm^2 SHJ solar cells using varying plasma powers (1800 - 1850 - 1900 - 1950 - 2000 - 2050 W), and their respective cell performances were examined. The optoelectronic characteristics of the fabricated ITO films were explored within the wavelength range of 300-1200 nm. The primary objective of this investigation was to enhance the power conversion efficiency (PCE) of SHJ solar cells by augmenting light absorption and minimizing light reflection. Subsequently, the performances of the ITO films, deposited using different plasma powers SHJ solar cells, were evaluated, resulting in the highest achieved conversion efficiency (η) of 17.03%.

2. MATERIAL AND METHOD

2.1. Thin Film Deposition

ITO films were deposited onto soda-lime glass substrates (surface: 2.5 x 2.5 cm^2, thickness: 1.1 mm) through sputtering using a DC magnetron (13.56 MHz) integrated into a PVD system. Figure 1 illustrates the schematic representation of the PVD setup. For the production of ITO films, a sputtering target with 99.999% (5N) purity of ITO was employed. The resulting films had a thickness of approximately 100 nm. Before introducing the glass substrates into the PVD chamber, a meticulous cleaning procedure was performed. Each glass substrate was subjected to a sequential cleaning regimen, involving a 5-minute immersion in acetone within an ultrasonic bath, followed by an additional 5-minute immersion in ethanol, and concluded with a 10-minute immersion in distilled water. Afterward, they were dried using Nitrogen (N_2) gas. The cleaned glass substrates were then placed within the PVD system and kept until a working pressure of $1x10^{-6}$ mbar was attained. The pressure within the PVD was maintained at $2x10^{-2}$ mbar using a continuous supply of Argon (Ar) gas and Oxygen (O_2). To prevent system contamination, an initial empty run was performed before loading the substrates into the system for the deposition process. The deposition parameters utilized for the fabrication of the ITO films are outlined in Table 1.

Table 1. Deposition parameters of ITO films.

Deposition Parameters	ITO
Base pressure (mbar)	$1x10^{-6}$
Deposition Pressure (mbar)	$2x10^{-2}$
Ar (sccm)	200
O_2 (sccm)	3.3
Temperature (°C)	200
Plasma Power (W)	1800-1850-1900-1950-2000-2050

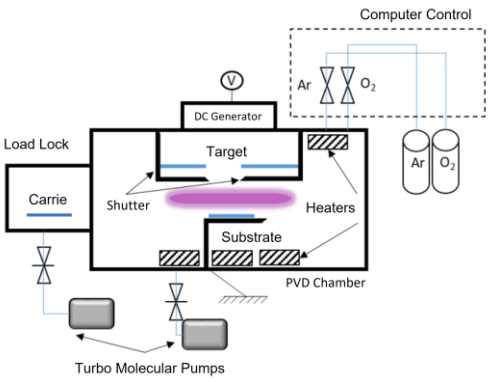

Figure 1. Schematic illustration of the PVD system.

2.2. Production of Silicon Heterojunction Solar Cells (SHJ)

In the second phase of this study, SHJ solar cells were fabricated using 5x5 cm^2, 180 µm thick, (100) orientation random pyramid textured c-Si substrates. To prepare the substrates, the oxide layer on the c-Si surface was eliminated using a hydrofluoric acid (HF) solution, followed by rinsing with distilled water and drying with N_2. Next, 10 nm thick hydrogenated amorphous silicon (a-Si:H (i)) layers were deposited on both surfaces of the c-Si substrate using the plasma-enhanced chemical vapor deposition (PECVD) method, utilizing silane (SiH_4) and hydrogen (H_2) gases. Subsequently, a 10 nm thick p-type a-Si layer (SiH_4, H_2, and Trimethyl boron (TMB) gas) was deposited on the front surface, while a 10 nm thick n-type a-Si layer (SiH_4, H_2, and Phosphine (PH_3) gas) was deposited on the back surface. On the rear surface of the n-type a-Si:H layer, consecutive layers of 40 nm ITO and 220 nm silver (Ag) were deposited using PVD. The thickness of the ITO and Ag layers was kept constant across all SHJ solar cells. For the front surface, the deposition of the ITO layer was performed on the p-type a-Si:H layer utilizing different plasma powers. Using various plasma powers, the ITO layer was deposited on the front surface of the p-type a-Si:H layer with a thickness of 100 nm. Figure 2 illustrates the fabricated SHJ solar cell structure. Ultimately, the front surface of the solar cells underwent metallization using Ag paste through the screen-printing method.

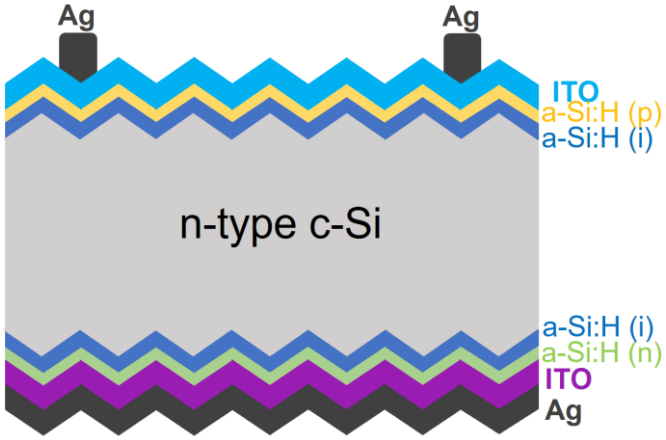

Figure 2. Schematic representation of the SHJ solar cell.

2.3. Characterization

In this study, optical, electrical, and structural parameters of ITO films were investigated. The structural properties of the ITO films were investigated using a Pan analytical-XRD device with CuKα radiation (λ=0.15418 nm) through X-ray diffraction. The determination of the thickness and optical characteristics of the thin films was carried out utilizing a Woollam V-Vase Ellipsometer, specifically within the wavelength range spanning from 300 to 1200 nm. The electrical properties of the ITO films were assessed using a contactless sheet resistance system (EddyCus® TF lab 4040 Hybrid). Furthermore, the efficiency performance of the solar cell was evaluated using the Sinton Suns-Voc WCP-120 device.

3. RESULTS AND DISCUSSION

3.1 Structural and Morphological Features

The structural properties of ITO films were investigated using X-ray diffraction method. X-ray diffraction method allows the examination of crystal structures by creating constructive and destructive interferences as a result of X-rays striking the parallel planes of atoms. In this method, the angle θ is determined for the strongest constructive interference for X-rays using Bragg's Law [31].

$$2d_{hkl}sin\theta = n\lambda \quad (1)$$

Parameters such as the distance (d) between planes of the crystal lattice, the Bragg angle (θ), an integer (n) representing the order of the diffraction peak, and the X-ray wavelength (λ) are used. Miller indices (h, k, l) of crystallographic planes are also taken into account. The calculation of the crystallite size (D) of the ITO thin films was conducted employing the Debye-Scherrer equation [32].

$$D = \frac{k\lambda}{\beta \cos\theta} \tag{2}$$

In this context, k represents the shape factor (0.9), λ the X-ray wavelength, and β the broadening of the diffraction line peak at an angle of 2θ at the full-width half-maximum (FWHM) in radians measured using the Gaussian distribution. The symbol θ represents the Bragg angle.

In this study, the XRD method was employed to analyze the crystal structure of ITO films deposited under various plasma powers (1800, 1850, 1900, 1950, 2000, and 2050 W). The scanning range for 2θ was set between 10° and 80°, and the outcomes obtained are illustrated in Figure 3. Based on the analysis results, all the deposited films exhibited polycrystalline characteristics, and the diffraction peaks (211), (222), (400), (440), and (622) indicated a cubic ITO structure (ICSD Card No. 98-005-0849) [33], [34]. The crystallinity of the ITO films was found to be influenced by the fabrication method and deposition conditions. While the films deposited at 1800 W did not exhibit (400) and (622) diffraction peaks, these peaks were observed with plasma powers exceeding 1850 W (Figure 3). This suggests that the plasma power enhances atomic arrangement, leading to an improved crystal structure. Table 2 presents the structural parameters of the ITO films deposited under different plasma powers, with these parameters calculated relative to the diffraction peak plane of highest intensity (222). According to this plane, the FWHM value of the ITO film deposited at 2050 W was determined to be the lowest (7.3E-03 rad). Conversely, the ITO film deposited at 1950 W exhibited the highest FWHM value (8.0E-03 rad). Furthermore, the 2θ values corresponding to the orientation of the ITO films (222) deposited at 1800, 1850, 1900, 1950, 2000, and 2050 W were measured as 30.21°, 30.19°, 30.22°, 29.95°, 30.21°, and 30.20°, respectively. In addition, the energy of the ions during sputtering may affect the preferred orientation of the crystalline particles because of these shifts in 2θ values. Higher sputtering powers may favor the growth of certain crystal planes, causing a shift in 2θ values [35], [36].

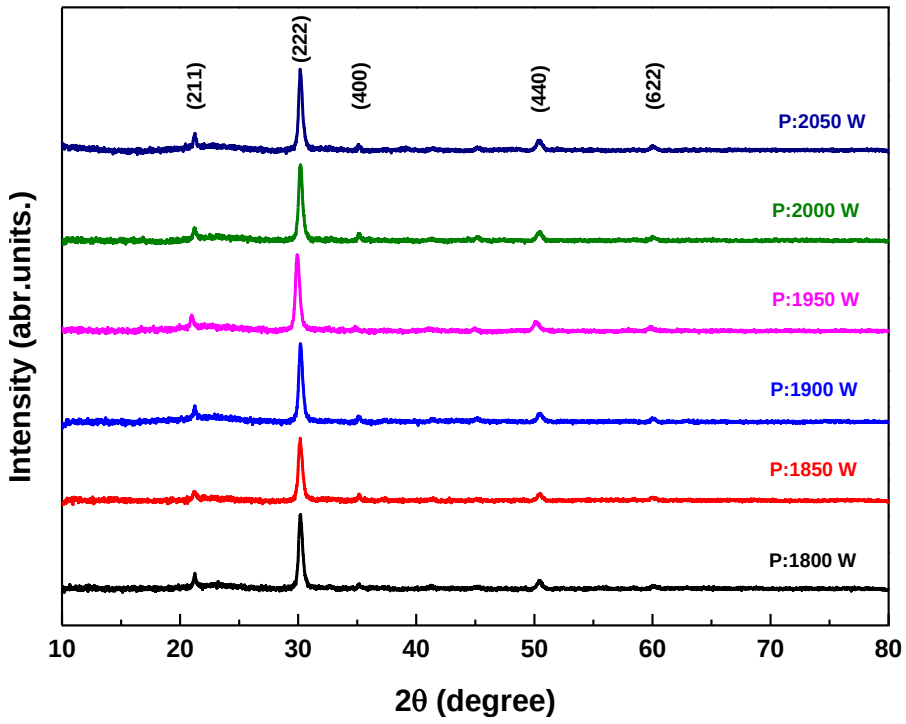

Figure 3. XRD patterns of ITO films deposited on the glass surface at 1800, 1850, 1900, 1950, 2000, and 2050 W plasma power.

The crystallite size and FWHM values of the ITO films generated under different plasma powers are presented in Table 2, and the crystallite size was determined using equation (2). A notable inverse relationship was observed between the crystallite size and FWHM values, where an increase in crystallite size corresponded to a significant decrease in FWHM (as depicted in Figure 4). Moreover, Table 2 demonstrates that the ITO films deposited at 1850 and 1950 W exhibited lower crystallite sizes (18 nm) compared to the films deposited at the same value and other plasma powers. The ITO films deposited at 1800, 1900, 2000, and 2050 W displayed the best crystallite sizes (19 nm). This outcome indicates that the ITO samples exhibit an improved crystal structure at plasma powers of 1800, 1900, 2000, and 2050 W. However, it is worth noting that the values are quite close to each other.

Table 2. FWHM (β), Bragg angle (θ), and crystallite size (D) values of ITO films deposited at 1800, 1850, 1900, 1950, 2000, and 2050 W plasma power.

Power (W)	β (rad)	θ (degres)	cosθ	D (nm)
1800	7.6E-03	15.1046	0.9655	19
1850	7.9E-03	15.0948	0.9655	18
1900	7.4E-03	15.1085	0.9654	19
1950	8.0E-03	14.9748	0.9660	18
2000	7.5E-03	15.1030	0.9655	19
2050	7.3E-03	15.1020	0.9655	19

3.2. Optical and Electrical Properties

Figures 4 and 5 depict the transmittance and reflection spectra, respectively, of the ITO films deposited on glass substrates through the PVD method, employing diverse plasma powers. A comprehensive summary of the optical properties, encompassing transmittance and reflection, of the films on the glass substrate is presented in Table 3. The transmittance spectra of the films exhibit remarkably high values within the visible region of the electromagnetic spectrum. Across the wavelength range of 400-700 nm, the ITO films deposited using different plasma powers demonstrated an average transmittance exceeding 78% and a reflectance below 18% (Table 3). Notably, the highest average transmittance of 81% was observed in the ITO film deposited at 2050 W, while the lowest transmittance was recorded in the ITO film deposited at 1800 W (77%). With an increase in plasma power, the transmittance showed an upward trend at lower wavelengths (400-700 nm), but conversely declined at higher wavelengths. Among the ITO films deposited using different plasma powers, the one with the highest transmittance within the visible region was determined to be the film generated at 2050 W, as illustrated in Figure 4.

Table 3. Transmittance, reflection and energy band gaps of ITO films deposited at 1800, 1850, 1900, 1950, 2000 and 2050 W plasma power.

Power (W)	Average Transmittance (%) (400-700 nm)	Average Reflection (%) (400-700 nm)	Eg (eV)	Transmittance (%) (550 nm)
1800	77	18	3.91	76
1850	79	18	3.91	78
1900	80	15	3.90	79
1950	79	16	3.91	79
2000	80	16	3.91	80
2050	81	15	3.91	81

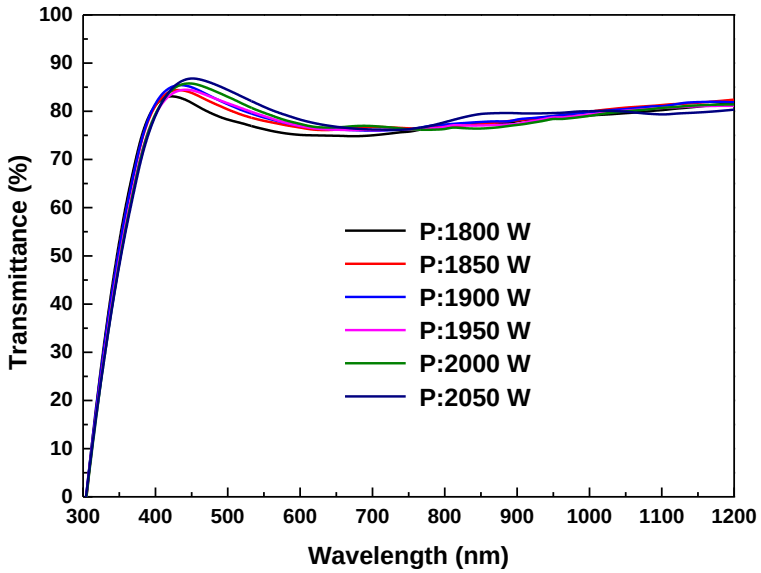

Figure 4. Transmission spectra of ITO films deposited at 1800, 1850, 1900, 1950, 2000, and 2050 W plasma power.

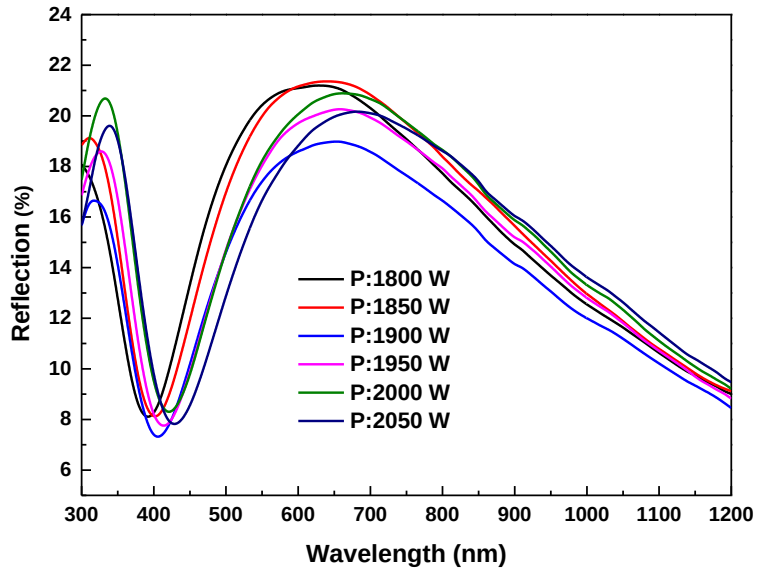

Figure 5. Reflection spectra of ITO films deposited at 1800, 1850, 1900, 1950, 2000, and 2050 W plasma power.

Figure 6 shows the graph hν corresponding to $(\alpha h\nu)^2$. The results were calculated using the bandgap measurement, Tauc plot derivative of ITO films deposited at different plasma powers [37]. The optical band gap values were determined as 3.90 eV for the film deposited at 1900 W, and as 3.91 eV for the remaining ITO films. The summary of the band gap energy values is provided in Table 3. From these findings, it can be observed that the plasma power had minimal influence on the band gap of the ITO films.

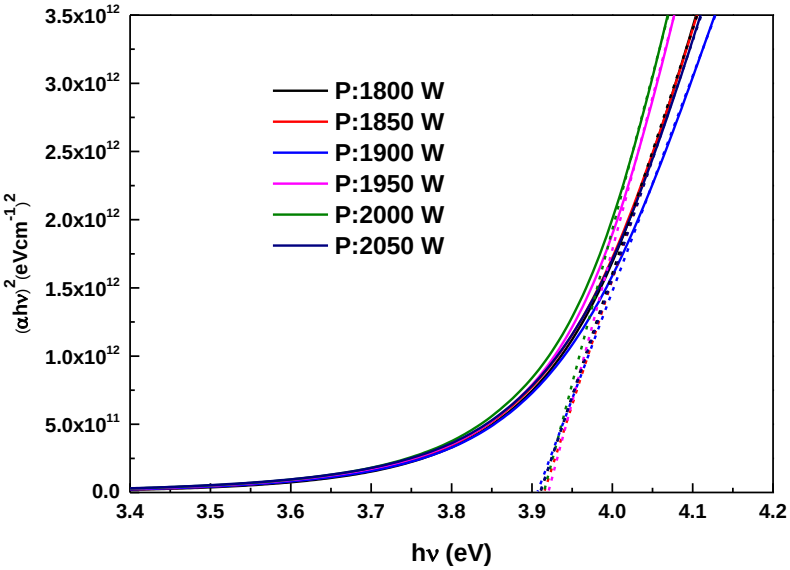

Figure 6. Graph of hν versus $(\alpha h\nu)^2$ for ITO films deposited at 1800, 1850, 1900, 1950, 2000, and 2050 W plasma power.

The transmittance values at a wavelength of 550 nm are provided in Table 3 to calculate the Figure of Merit (FOM) for ITO films deposited under different plasma powers. By utilizing the transmittance and sheet resistance properties of the ITO films at this specific wavelength, the FOM (ϕ_{TC}) values were calculated using equation (3). Figure 7 displays the obtained ϕ_{TC} and R_{sh} values for the ITO films deposited with varying plasma powers. It was observed that ϕ_{TC} values increased as the plasma power increased across all films. The ITO film deposited at 2050 W exhibited the highest FOM value of 1.87×10^{-3} Ohm $^{-1}$. Furthermore, Figure 7 also presents the R_{sh} values for the ITO films deposited under different plasma powers. The film deposited at 1800 W displayed the highest R_{sh} value of 78.7 Ω/sq, whereas the film deposited at 2050 W demonstrated the lowest R_{sh} value of 64.9 Ω/sq. It can be noted that there is a consistent decrease in R_{sh} values with the increase in plasma power. These findings indicate that the plasma power enhances the electrical properties of the material.

$$\Phi_{TC} = T^{10}/R_{sh} \tag{3}$$

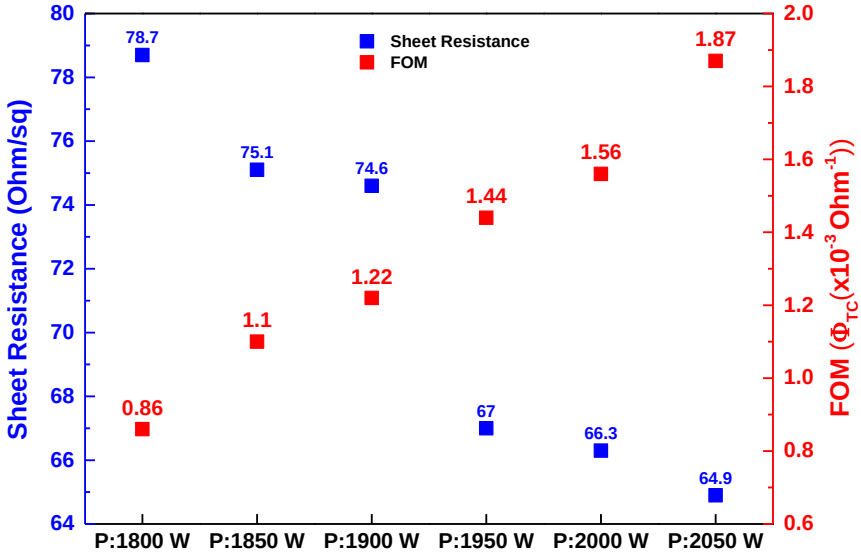

Figure 7. FOM and sheet resistance graph of ITO films deposited at 1800, 1850, 1900, 1950, 2000, and 2050 W plasma power.

The photovoltaic parameters of SHJ solar cells are provided in Table 4. Among all the plasma powers used, the ITO film deposited at 2050 W demonstrated superior performance in terms of high optical properties and low layer resistance, resulting in high efficiency. The SHJ solar cell utilizing the ITO layer deposited at 2050 W exhibited parameters of 0.613 V, 79.1%, and 17.03% for V_{OC}, FF, and η, respectively. On the other hand, the SHJ solar cell fabricated using the ITO layer deposited at 1800 W showed lower efficiency due to its lower optical properties and higher layer resistance. Increasing the plasma power resulted in higher V_{OC} and conversion efficiency in the solar cell. Figure 8 shows the current density-voltage (J-V) graph of the SHJ solar cell using ITO film deposited at 2050 W plasma power, showing its excellent performance as a TCO in the SHJ solar cell.

Table 4. Photovoltaic parameters of SHJ solar cells.

Plasma Power (W)	Voc (V)	J_{SC} (A/cm^2)	V_{MP} (V)	J_{MP} (A/cm^2)	FF (%)	Efficiency (η)
1800	0.565	0.035	0.476	0.032	77.8	15.38
1850	0.570	0.035	0.479	0.033	78.3	15.49
1900	0.587	0.035	0.497	0.032	78.6	16.14
1950	0.596	0.035	0.504	0.033	79.6	16.59
2000	0.602	0.035	0.509	0.033	78.5	16.56
2050	0.613	0.035	0.522	0.033	79.1	17.03

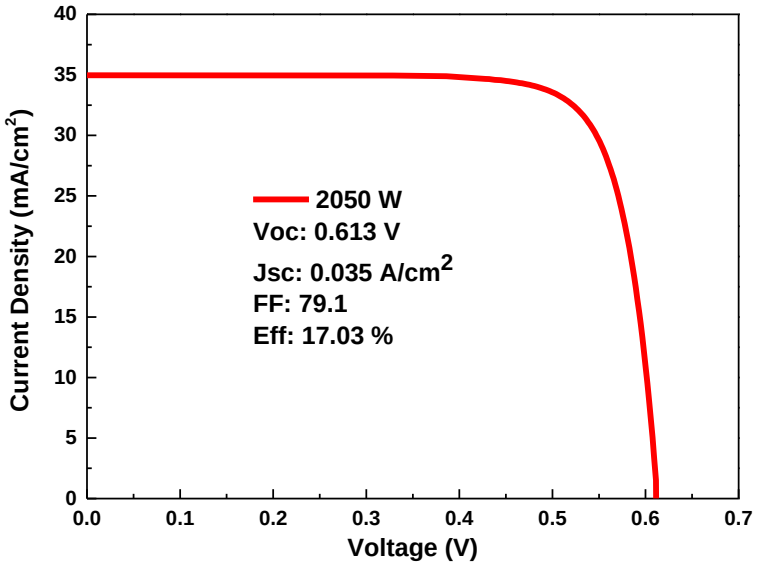

Figure 8. The current density-voltage (J-V) graph of the SHJ solar cell fabricated using ITO with a plasma power of 2050 W.

4. CONCLUSIONS

In this study, the structural, optical, and electrical properties of ITO films deposited by the DC magnetron sputtering method using different plasma powers (1800, 1850, 1900, 1950, 2000, and 2050 W) on 5x5 cm^2 n-type Si wafer at 200 °C were investigated. The optical properties were assessed by measuring the average transmittance values within the visible region (400-700 nm). The highest transmittance (81%) was observed in the ITO film deposited at 2050 W, followed by the ITO films deposited at 1900 W and 1950 W, which exhibited transmittance values of 80%. The lowest transmittance (77%) was observed in the ITO film deposited at 1800 W. The sheet resistance values were measured for all films, and the ITO film deposited at 2050 W exhibited the lowest sheet resistance (64.9 Ω/sq). Additionally, the FOM value for this film was calculated to be 1.87x10^{-3} Ohm^{-1}, indicating its superior electrical performance compared to films deposited at other plasma powers. The structural properties of the films were thoroughly examined through XRD analysis, unveiling the presence of distinct diffraction peaks corresponding to the crystal planes (211), (222), (400), (440), and (622) across all ITO films. Furthermore, the analysis revealed that the ITO films deposited at 1850 W and 1950 W exhibited crystallite sizes of 18 nm, whereas the films deposited at 1800 W,

1900 W, 2000 W, and 2050 W demonstrated crystallite sizes of 19 nm. Based on the analysis results, the ITO film deposited at 2050 W demonstrated the best overall performance among the different plasma powers. Finally, a remarkable efficiency of 17.03% was achieved in the SHJ solar cell utilizing the ITO film deposited at 2050 W.

SIMILARITY RATE: 15 %

ACKNOWLEDGEMENT

The authors gratefully acknowledge the funding from The Scientific and Technological Research Council of Turkey (TÜBITAK-20AG014).

REFERENCES

[1] C. Battaglia, A. Cuevas, and S. de Wolf, "High-efficiency crystalline silicon solar cells: status and perspectives," *Energy Environ Sci*, vol. 9, no. 5, pp. 1552–1576, 2016, doi: 10.1039/C5EE03380B.

[2] S. Q. Hussain *et al.*, "Highly transparent RF magnetron-sputtered indium tin oxide films for a-Si:H/c-Si heterojunction solar cells amorphous/crystalline silicon," *Mater Sci Semicond Process*, vol. 24, pp. 225–230, 2014, doi: https://doi.org/10.1016/j.mssp.2014.02.044.

[3] M. Taguchi, "Review—Development History of High Efficiency Silicon Heterojunction Solar Cell: From Discovery to Practical Use," *ECS Journal of Solid State Science and Technology*, vol. 10, no. 2, p. 025002, 2021, doi: 10.1149/2162-8777/abdfb6.

[4] M. A. Green, E. D. Dunlop, J. Hohl-Ebinger, M. Yoshita, N. Kopidakis, and A. W. Y. Ho-Baillie, "Solar cell efficiency tables (Version 55)," *Progress in Photovoltaics: Research and Applications*, vol. 28, no. 1, pp. 3–15, Jan. 2020, doi: https://doi.org/10.1002/pip.3228.

[5] S. de Wolf, A. Descoeudres, Z. C. Holman, and C. Ballif, "High-efficiency Silicon Heterojunction Solar Cells: A Review," *Green*, vol. 2, no. 1, pp. 7–24, 2012, doi: doi:10.1515/green-2011-0018.

[6] V. Singh, C. K. Suman, and S. Kumar, "Indium Tin Oxide (ITO) films on flexible substrates for organic light emitting diodes," in *Proc. of ASID*, 2006, p. 388.

[7] B. Walker, A. K. Pradhan, and B. Xiao, "Low temperature fabrication of high performance ZnO thin film transistors with high-k dielectrics," *Solid State Electron*, vol. 111, pp. 58–61, 2015, doi: https://doi.org/10.1016/j.sse.2015.05.004.

[8] Y. Zhang *et al.*, "Flexible transparent high-voltage diodes for energy management in wearable electronics," *Nano Energy*, vol. 40, pp. 289–299, 2017, doi: https://doi.org/10.1016/j.nanoen.2017.08.025.

[9] N. Cheng, Y. Shao, J. Liu, and X. Sun, "Electrocatalysts by atomic layer deposition for fuel cell applications," *Nano Energy*, vol. 29, pp. 220–242, 2016, doi: https://doi.org/10.1016/j.nanoen.2016.01.016.

[10] B. Yan, G. Yue, J. M. Owens, J. Yang, and S. Guha, "Light-induced metastability in hydrogenated nanocrystalline silicon solar cells," *Appl Phys Lett*, vol. 85, no. 11, pp. 1925–1927, Sep. 2004, doi: 10.1063/1.1790072.

[11] C. G. Granqvist, "Transparent conductors as solar energy materials: A panoramic review," *Solar Energy Materials and Solar Cells*, vol. 91, no. 17, pp. 1529–1598, 2007, doi: https://doi.org/10.1016/j.solmat.2007.04.031.

[12] Y.-H. Tak, K.-B. Kim, H.-G. Park, K.-H. Lee, and J.-R. Lee, "Criteria for ITO (indium–tin-oxide) thin film as the bottom electrode of an organic light emitting diode," *Thin Solid Films*, vol. 411, no. 1, pp. 12–16, 2002, doi: https://doi.org/10.1016/S0040-6090(02)00165-7.

[13] M. K. M. Ali, K. Ibrahim, O. S. Hamad, M. H. Eisa, M. G. Faraj, and F. Azhari, "Deposited indium tin oxide (ITO) thin films by dc-magnetron sputtering on polyethylene terephthalate substrate (PET)," *Rom. J. Phys*, vol. 56, no. 5–6, pp. 730–741, 2011.

[14] C. S. Moon and J. G. Han, "Low temperature synthesis of ITO thin film on polymer in Ar/H2 plasma by pulsed DC magnetron sputtering," *Thin Solid Films*, vol. 516, no. 19, pp. 6560–6564, 2008, doi: https://doi.org/10.1016/j.tsf.2007.11.028.

[15] S. Laux, N. Kaiser, A. Zöller, R. Götzelmann, H. Lauth, and H. Bernitzki, "Room-temperature deposition of indium tin oxide thin films with plasma ion-assisted evaporation," *Thin Solid Films*, vol. 335, no. 1, pp. 1–5, 1998, doi: https://doi.org/10.1016/S0040-6090(98)00861-X.

[16] D. C. Paine, T. Whitson, D. Janiac, R. Beresford, C. O. Yang, and B. Lewis, "A study of low temperature crystallization of amorphous thin film indium–tin–oxide," *J Appl Phys*, vol. 85, no. 12, pp. 8445–8450, May 1999, doi: 10.1063/1.370695.

[17] T. Karasawa and Y. Miyata, "Electrical and optical properties of indium tin oxide thin films deposited on unheated substrates by d.c. reactive sputtering," *Thin Solid Films*, vol. 223, no. 1, pp. 135–139, 1993, doi: https://doi.org/10.1016/0040-6090(93)90737-A.

[18] L. Meng and M. P. dos Santos, "Properties of indium tin oxide films prepared by rf reactive magnetron sputtering at different substrate temperature," *Thin Solid Films*, vol. 322, no. 1, pp. 56–62, 1998, doi: https://doi.org/10.1016/S0040-6090(97)00939-5.

[19] D. Raoufi, A. Kiasatpour, H. R. Fallah, and A. S. H. Rozatian, "Surface characterization and microstructure of ITO thin films at different annealing temperatures," *Appl Surf Sci*, vol. 253, no. 23, pp. 9085–9090, 2007, doi: https://doi.org/10.1016/j.apsusc.2007.05.032.

[20] L. Raniero *et al.*, "Role of hydrogen plasma on electrical and optical properties of ZGO, ITO and IZO transparent and conductive coatings," *Thin Solid Films*, vol. 511–512, pp. 295–298, 2006, doi: https://doi.org/10.1016/j.tsf.2005.12.057.

[21] S. M. Kim, H.-W. Choi, K.-H. Kim, S.-J. Park, and H.-H. Yoon, "Preparation of ITO and IZO thin films by using the facing targets sputtering (FTS) method," *J. Korean Phys. Soc*, vol. 55, no. 5, pp. 1996–2001, 2009, [Online]. Available: http://dx.doi.org/10.3938/jkps.55.1996

[22] T. J. Burke and C. Segrin, "Examining Diet- and Exercise-Related Communication in Romantic Relationships: Associations With Health Behaviors," *Health Commun*, vol. 29, no. 9, pp. 877–887, Oct. 2014, doi: 10.1080/10410236.2013.811625.

[23] J. Montero, C. Guillén, and J. Herrero, "AZO/ATO double-layered transparent conducting electrode: A thermal stability study," *Thin Solid Films*, vol. 519, no. 21, pp. 7564–7567, 2011, doi: https://doi.org/10.1016/j.tsf.2010.12.103.

[24] H. Park, J. Lee, H. Kim, D. Kim, J. Raja, and J. Yi, "Influence of SnO2:F/ZnO:Al bi-layer as a front electrode on the properties of p-i-n amorphous silicon based thin film solar cells," *Appl Phys Lett*, vol. 102, no. 19, p. 191602, May 2013, doi: 10.1063/1.4807127.

[25] M. P. Taylor *et al.*, "The Remarkable Thermal Stability of Amorphous In-Zn-O Transparent Conductors," *Adv Funct Mater*, vol. 18, no. 20, pp. 3169–3178, Oct. 2008, doi: https://doi.org/10.1002/adfm.200700604.

[26] R. Riveros, E. Romero, and G. Gordillo, "Synthesis and characterization of highly transparent and conductive SnO2: F and In2O3: Sn thin films deposited by spray pyrolysis," *Brazilian journal of physics*, vol. 36, pp. 1042–1045, 2006.

[27] A. Ambrosini, A. Duarte, K. R. Poeppelmeier, M. Lane, C. R. Kannewurf, and T. O. Mason, "Electrical, Optical, and Structural Properties of Tin-Doped In2O3–M2O3 Solid Solutions (M=Y, Sc)," *J Solid State Chem*, vol. 153, no. 1, pp. 41–47, 2000, doi: https://doi.org/10.1006/jssc.2000.8737.

[28] J. M. Gaskell and D. W. Sheel, "Deposition of indium tin oxide by atmospheric pressure chemical vapour deposition," *Thin Solid Films*, vol. 520, no. 12, pp. 4110–4113, 2012, doi: https://doi.org/10.1016/j.tsf.2011.04.191.

[29] M. J. Alam and D. C. Cameron, "Optical and electrical properties of transparent conductive ITO thin films deposited by sol–gel process," *Thin Solid Films*, vol. 377–378, pp. 455–459, 2000, doi: https://doi.org/10.1016/S0040-6090(00)01369-9.

[30] A. H. Sofi, M. A. Shah, and K. Asokan, "Structural, Optical and Electrical Properties of ITO Thin Films," *J Electron Mater*, vol. 47, no. 2, pp. 1344–1352, 2018, doi: 10.1007/s11664-017-5915-9.

[31] D.-W. Kim and D.-W. Park, "Preparation of indium tin oxide (ITO) nanoparticles by DC arc plasma," *Surf Coat Technol*, vol. 205, pp. S201–S205, 2010, doi: https://doi.org/10.1016/j.surfcoat.2010.07.078.

[32] A. H. Sofi and M. A. Shah, "Structural and electrical properties of copper doped In2O3 nanostructures prepared by citrate gel processes," *Mater Res Express*, vol. 6, no. 4, p. 045039, 2019, doi: 10.1088/2053-1591/aafc0b.

[33] S.-Y. Lien, "Characterization and optimization of ITO thin films for application in heterojunction silicon solar cells," *Thin Solid Films*, vol. 518, no. 21, Supplement, pp. S10–S13, 2010, doi: https://doi.org/10.1016/j.tsf.2010.03.023.

[34] T. Ogi, D. Hidayat, F. Iskandar, A. Purwanto, and K. Okuyama, "Direct synthesis of highly crystalline transparent conducting oxide nanoparticles by low pressure spray pyrolysis," *Advanced Powder Technology*, vol. 20, no. 2, pp. 203–209, 2009, doi: https://doi.org/10.1016/j.apt.2008.09.002.

[35] W.-F. Wu, B.-S. Chiou, and S.-T. Hsieh, “Effect of sputtering power on the structural and optical properties of RF magnetron sputtered ITO films,” vol. 9, no. 6, pp. 1242–1249, Jun. 1994, doi: https://doi.org/10.1088/0268-1242/9/6/014.

[36] A. Mansingh and V. Kumar, “Properties of RF-sputtered ITO films on substrates above and below the virtual source,” vol. 22, no. 3, pp. 455–457, Mar. 1989, doi: https://doi.org/10.1088/0022-3727/22/3/013.

[37] Tauc, "Optical properties and electronic structure of amorphous Ge and Si," Materials research bulletin, vol. 3, no. 1 second. 37-46, 1968, doi: https://doi.org/10.1016/0025-5408(68)90023-8